# Mechanistic analysis of cavitation assisted transesterification on biodiesel characteristics

Baharak Sajjadi, A.R. Abdul Aziz *, Shaliza Ibrahim

*Department of Chemical Engineering, Faculty of Engineering, University of Malaya, 50603 Kuala Lumpur, Malaysia*

ARTICLE INFO

*Article history:*
Received 6 December 2013
Received in revised form 2 June 2014
Accepted 8 June 2014
Available online 20 June 2014

*Keywords:*
Biodiesel
Ultrasound
Transesterification
Mechanical stirring
Biodiesel properties
Cavitaion

ABSTRACT

The influence of sonoluminescence transesterification on biodiesel physicochemical properties was investigated and the results were compared to those of traditional mechanical stirring. This study was conducted to identify the mechanistic features of ultrasonication by coupling statistical analysis of the experiments into the simulation of cavitation bubble. Different combinations of operational variables were employed for alkali-catalysis transesterification of palm oil. The experimental results showed that transesterification with ultrasound irradiation could change the biodiesel density by about 0.3 kg/m$^3$; the viscosity by 0.12 mm$^2$/s; the pour point by about 1–2 °C and the flash point by 5 °C compared to the traditional method. Furthermore, 93.84% of yield with alcohol to oil molar ratio of 6:1 could be achieved through ultrasound assisted transesterification within only 20 min. However, only 89.09% of reaction yield was obtained by traditional macro mixing/heating under the same condition. Based on the simulated oscillation velocity value, the cavitation phenomenon significantly contributed to generation of fine micro emulsion and was able to overcome mass transfer restriction. It was found that the sonoluminescence bubbles reached the temperature of 758–713 K, pressure of 235.5–159.55 bar, oscillation velocity of 3.5–6.5 cm/s, and equilibrium radius of 17.9–13.7 times greater than its initial size under the ambient temperature of 50–64 °C at the moment of collapse. This showed that the sonoluminescence bubbles were in the condition in which the decomposition phenomena were activated and the reaction rate was accelerated together with a change in the biodiesel properties.



## 1. Introduction

Among the biofuels currently in use or researched, Free Fatty Acid Methyl Esters (FAME), which is also known as biodiesel is considered an ideal alternative to diesel due to their similarities and advantages [1]. Biodiesel is commonly generated through a three-step, consecutive and reversible reaction called "transesterification". Low mass transfer due to immiscible nature of reactants is the main weakness of transesterification [2,3]. Recently, ultrasound assisted transesterification has been confirmed as a green synthesis method that is fast and energy-efficient [4]. It is due to the ultrasound ability to enhance mass transfer between the immiscible reactants. In other words, ultrasound waves are sinusoidal mechanistic waves consisting of both expansion (negative) and compression (positive) pressure waves. Hence, irradiation of ultrasound waves generates vacuum micro-regions in the liquid called "sonoluminescence bubble" that are filled with reactants vapors. Mass transfer goes efficiently inside the micro-fine bubbles. "Cavitation" happens when bubbles grow (expansion) and collapse (compression) intensively [5]. This phenomenon assists the system to generate fine micro-emulsion through generation of micro streams, micro turbulent eddies and shock waves. Besides, the collapse is extremely energetic, resulting in generation of highly pressurized and over-heated regions called "hot spots" which induce the reaction [6].

Many authors have reported that low frequency ultrasound accelerates reaction rate in which higher conversion is achieved in transesterification within shorter reaction time compared to the other approaches [7–9]. Thermal decomposition can also be carried out in parallel with transesterification within these bubbles. Highly volatile hydrophobic molecules can easily and directly decompose in hot spots. Generally, biodiesel starts to decompose upon thermal stressing at 275 °C and above. The decomposition mainly involves (i) dimerization or polymerization reactions that form higher molecular weight components; (ii) isomerization reactions that transfer unsaturated *cis*-type FAMEs to *trans*-type FAMEs and (iii) pyrolysis reactions that break down FAMEs to form lower molecular weight FAMEs and hydrocarbons. These reactions occur

* Corresponding author. Tel.: +60 379675300; fax: +60 379675319.
*E-mail address:* azizraman@um.edu.my (A.R. Abdul Aziz).

http://dx.doi.org/10.1016/j.ultsonch.2014.06.004
1350-4177/

at 300–425 °C, 275–400 °C and >350 °C, respectively [10]. Bruno and co-workers [11] observed that the polymerization and cracking of unsaturated FAMEs significantly influenced the volatility of biodiesel fuel. Imahara et al. [12] found that the cold flow properties of biodiesel produced under high temperature and pressure (350 °C and 43 MPa) increased slightly due to *cis–trans* isomerization. Lin et al. [10] investigated the influence of thermal stressing on biodiesel viscosity and cold flow properties at 250–425 °C. They demonstrated that *cis–trans* isomerization reactions had a minimal effect on biodiesel characteristics. Meanwhile, pyrolysis reactions reduced both viscosity and the crystallization onset temperature but polymerization showed the opposite effects. Xin et al. [13] observed that the oxidation stability of biodiesel made from waste cooking oils with high peroxide values was improved at temperature of 270 °C and pressure of 17 MPa compared to biodiesel produced from the same feedstock by conventional method at lower temperature and pressure.

Based on a detailed review done by Veljković et al. [6], despite a large quantity of researches on intensification of transesterification under irradiation of ultrasound energy, the quality of biodiesel produced in such conditions have not been well addressed. These characteristics influence flow injection and atomization of fuel as well as energy content of engine and its safety. In the current study, the authors tried to identify the physical mechanism of cavitation and provide a deep insight into the sonoluminescence transesterification that form conditions that may activate the thermal decomposition phenomena and influence the biodiesel characteristics. The principle aim is to find a link between the influence of thermal stressing and quality of biodiesel produced from alkaline transesterification of palm oil under ultrasound irradiation.

## 2. Methodology

### 2.1. Material and method

RBD (Refined, Bleached and Deodorized) palm oil was employed as the source of triglyceride. Its chemical composition and physical properties can be found in Table 1. Absolute methanol (99.99%) and hydrochloric acid (30 wt.%) for the pre-treatment step were purchased from Sigma Aldrich while potassium hydroxide pellets (99.99 wt.%) were purchased from Merck Companies, Malaysia. A mixture of fatty acid including palmitic, stearic, oleic, linolenic and linoleic methyl esters (called MSTFA) which was used as the HPLC standards in this study, was supplied by Supelco Company.

### 2.2. Experimental design

Central composite design (CCD) was employed to specify the effects of operational variables on conversion of oil to FAME. This type of design is desirable for sequential experiments to obtain proper information for examining lack of fit without a large number of design points [14]. The operational parameters included (i) temperature, in the range of 50–64 °C; (ii) MeOH:oil molar ratio, in the range of 6–12; (iii) concentration of catalyst, in the range of 1–2%; (iv) sonication power, in the range of 0–400 W; (v) mechanical stirring, in the range of 400–800 RPM and (vi) reaction time, in the range of 20–60 min. Each parameter was fixed and coded into levels: −1 (Minimum level), 0 (middle level) and +1 (Maximum level). Finally, 50 experimental runs including 10 axial points, 32 factorial points, and 1 replicable central point were designed. The central point was repeated 8 times in order to identify the experimental error. The employed design matrix with the related yield and biodiesel properties are reported in Tables 2 and 3 respectively.

**Table 1**
Properties of used palm oil.

| Property | Value |
|---|---|
| Density at 15 °C | 791.8 kg/m$^3$ |
| Viscosity at 40 °C | 33.60 mm$^2$ s$^{-1}$ |
| Moisture content (%) | 400 × 10$^{-6}$ ppm |
| Acid value | 51.8 ppm |
| Iodine value | 0.151 mg/g |

### 2.3. Biodiesel synthesis

A 300 ml stainless steel and a 400 ml glass flask were used as the reaction vessels. Both were equipped with a water bath to control the temperature; a condenser to inhibit the exhaust of evaporated methanol and a thermometer to record the reaction temperature. The sonication was carried out by a 24 kHz-ultrasonic processor, UP400S (Hielscher Ultrasonics). The mechanical stirring was done by an overhead stirrer (13516 IKA Eurostar 60 Digital). Both reactors were connected to a 220 V voltage regulator. Since ultrasonication generates heat, the temperature in the ultrasonic bath was controlled at about 2–10 °C below the reaction temperature.

The reactors were initially charged with favorable amount of palm oil and then heated to reaction temperature by the surrounding water. In the next step, a pre-provided and pre-heated solution of methanol and catalyst was added to the oil. Then, the stirring/sonication of the reaction started immediately and continued with the specified mixing intensity/sonication power and reaction time. After the stirring/sonification, the mixture was transferred to a separatory funnel for gravitational separation for 48 h. The methyl ester was then washed with diluted hydrochloric acid to neutralize the remaining alkaline catalyst before being washed by distilled water twice. Finally, the excessive methanol and water in the product were removed by rotary evaporation at 70 °C for 120 min.

### 2.4. Biodiesel analysis and characterization

The chemical compositions of biodiesel product and yield of reaction were determined by a gas chromatography (Agilent Technology gas chromatograph model GC 6890) equipped with cool-on column (DB-23, 60 mL, 0.250 mm ID, 0.15 μm film thickness). The results are summarised in Table 2. Helium was used as a carrier gas at the flow rate of 1.0 mL/min; nitrogen was used as a make-up gas at the flow rate of 25 mL/min and hydrogen was used as a fuel gas at the flow rate of 40 mL/min. The start-up temperature was 323 K, which was increased to 448 K at 25 K/min and further increased to 553 K at 5 K/min. 553 K was maintained for 5 min. The standard test methods according to ASTM Standard are applied to evaluate the quality of biodiesel [15]. The density of the biodiesel produced was analyzed (based on ASTM D4052-96) by a fully automatic density meter (Mettler Toledo model DM.40, *Switzerland*). The viscosity (based on ASTM D445-06) was measured by a fully automatic viscometer (Brookfield DV-II+PRO Viscometer). The pour and cloud point (based on ASTM D97-93 and D2500) were determined by a pour/cloud point tester (Normalab, model NTE 450, France) while flash point (based on ASTM D93-07) was determined by a Pensky–Martens Closed Cup Tester.

## 3. Mathematical model

The dynamic of sonoluminescence bubble along with the phenomena of liquid vaporization, diffusion, heat transfer and chemical reactions within the cavitation bubbles were simulated using Matlab to get a quantitative insight of the influence of ultrasound irradiation on a system (Mathworks Inc., USA).

**Table 2**
Experimental design matrix and the values of related Macro/Micro reaction yield.

| Run | Type | Temp (°C) | Oil Molar ratio | Cat wt.% | Mixing Watt (Micro) | Intensity RPM (Macro) | Time Minutes | Yield %(Micro) | Yield %(Macro) |
|---|---|---|---|---|---|---|---|---|---|
| 1 | Factorial | 50 | 6 | 1 | 300 | 400 | 20 | 86.99 | 81.60 |
| 2 | Factorial | 64 | 6 | 1 | 300 | 400 | 20 | 88.17 | 84.27 |
| 3 | Factorial | 50 | 12 | 1 | 300 | 400 | 20 | 88.94 | 84.93 |
| 4 | Factorial | 64 | 12 | 1 | 300 | 400 | 20 | 90.28 | 86.33 |
| 5 | Factorial | 50 | 6 | 2 | 300 | 400 | 20 | 91.44 | 83.49 |
| 6 | Factorial | 64 | 6 | 2 | 300 | 400 | 20 | 92.63 | 86.85 |
| 7 | Factorial | 50 | 12 | 2 | 300 | 400 | 20 | 91.92 | 86.41 |
| 8 | Factorial | 64 | 12 | 2 | 300 | 400 | 20 | 92.57 | 89.47 |
| 9 | Factorial | 50 | 6 | 1 | 400 | 800 | 20 | 89.20 | 82.82 |
| 10 | Factorial | 64 | 6 | 1 | 400 | 800 | 20 | 91.26 | 87.90 |
| 11 | Factorial | 50 | 12 | 1 | 400 | 800 | 20 | 90.35 | 85.96 |
| 12 | Factorial | 64 | 12 | 1 | 400 | 800 | 20 | 91.26 | 89.12 |
| 13 | Factorial | 50 | 6 | 2 | 400 | 800 | 20 | 91.19 | 86.89 |
| 14 | Factorial | 64 | 6 | 2 | 400 | 800 | 20 | 93.84 | 89.09 |
| 15 | Factorial | 50 | 12 | 2 | 400 | 800 | 20 | 93.75 | 87.34 |
| 16 | Factorial | 64 | 12 | 2 | 400 | 800 | 20 | 93.05 | 89.16 |
| 17 | Factorial | 50 | 6 | 1 | 300 | 400 | 60 | 89.92 | 87.12 |
| 18 | Factorial | 64 | 6 | 1 | 300 | 400 | 60 | 91.91 | 88.11 |
| 19 | Factorial | 50 | 12 | 1 | 300 | 400 | 60 | 91.61 | 88.74 |
| 20 | Factorial | 64 | 12 | 1 | 300 | 400 | 60 | 93.13 | 90.03 |
| 21 | Factorial | 50 | 6 | 2 | 300 | 400 | 60 | 91.88 | 87.99 |
| 22 | Factorial | 64 | 6 | 2 | 300 | 400 | 60 | 95.81 | 90.50 |
| 23 | Factorial | 50 | 12 | 2 | 300 | 400 | 60 | 91.26 | 88.72 |
| 24 | Factorial | 64 | 12 | 2 | 300 | 400 | 60 | 93.70 | 92.43 |
| 25 | Factorial | 50 | 6 | 1 | 400 | 800 | 60 | 90.89 | 90.24 |
| 26 | Factorial | 64 | 6 | 1 | 400 | 800 | 60 | 93.39 | 91.75 |
| 27 | Factorial | 50 | 12 | 1 | 400 | 800 | 60 | 92.27 | 90.67 |
| 28 | Factorial | 64 | 12 | 1 | 400 | 800 | 60 | 93.20 | 93.65 |
| 29 | Factorial | 50 | 6 | 2 | 400 | 800 | 60 | 89.74 | 91.01 |
| 30 | Factorial | 64 | 6 | 2 | 400 | 800 | 60 | 95.44 | 92.70 |
| 31 | Factorial | 50 | 12 | 2 | 400 | 800 | 60 | 92.81 | 91.31 |
| 32 | Factorial | 64 | 12 | 2 | 400 | 800 | 60 | 95.71 | 94.01 |
| 33 | Axial | 50 | 9 | 1.5 | 350 | 600 | 40 | 90.15 | 86.35 |
| 34 | Axial | 64 | 9 | 1.5 | 350 | 600 | 40 | 95.15 | 88.12 |
| 35 | Axial | 57 | 6 | 1.5 | 350 | 600 | 40 | 89.66 | 87.04 |
| 36 | Axial | 57 | 12 | 1.5 | 350 | 600 | 40 | 92.67 | 88.62 |
| 37 | Axial | 57 | 9 | 1 | 350 | 600 | 40 | 90.93 | 87.18 |
| 38 | Axial | 57 | 9 | 2 | 350 | 600 | 40 | 92.26 | 88.04 |
| 39 | Axial | 57 | 9 | 1.5 | 300 | 400 | 40 | 90.95 | 85.79 |
| 40 | Axial | 57 | 9 | 1.5 | 400 | 800 | 40 | 91.96 | 88.49 |
| 41 | Axial | 57 | 9 | 1.5 | 350 | 600 | 20 | 89.39 | 83.64 |
| 42 | Axial | 57 | 9 | 1.5 | 350 | 600 | 60 | 91.95 | 89.89 |
| 43 | Center | 57 | 9 | 1.5 | 350 | 600 | 40 | 91.11 | 87.08 |
| 44 | Center | 57 | 9 | 1.5 | 350 | 600 | 40 | 91.44 | 86.98 |
| 45 | Center | 57 | 9 | 1.5 | 350 | 600 | 40 | 91.90 | 87.18 |
| 46 | Center | 57 | 9 | 1.5 | 350 | 600 | 40 | 90.88 | 87.08 |
| 47 | Center | 57 | 9 | 1.5 | 350 | 600 | 40 | 91.53 | 87.13 |
| 48 | Center | 57 | 9 | 1.5 | 350 | 600 | 40 | 90.18 | 87.62 |
| 49 | Center | 57 | 9 | 1.5 | 350 | 600 | 40 | 90.80 | 86.49 |
| 50 | Center | 57 | 9 | 1.5 | 350 | 600 | 40 | 91.47 | 87.15 |

### 3.1. Bubble dynamics

The radial motion of the cavitation bubble is described by a variant of Rayleigh–Plesset equation [16], which takes into account the liquid compressibility:

$$\left(1-\frac{dR/dt}{c}\right)R\frac{d^2R}{dt^2}+\frac{3}{2}\left(1-\frac{dR/dt}{3c}\right)\left(\frac{dR}{dt}\right)^2 = \left(1-\frac{dR/dt}{c}\right)\frac{1}{\rho_L}(P_g-P_a-P_0)+\frac{R}{\rho_L c}\frac{dP_g}{R}-4v\frac{dR/dt}{R}-\frac{2\sigma}{\rho_L R} \quad (1)$$

where $\rho$, $\sigma$, $\mu$ are the density, surface tension coefficient and viscosity of the liquid. $c$ denotes the sound speed in the liquid; $P_0$ is the static pressure and $P_a$ is the acoustic driving pressure that can be explained by:

$$P_a = P_A \sin(\omega t) \quad (2)$$

where, $P_A = \sqrt{2\rho I_{US} c}$ and $\omega$ are the pressure amplitude and angular velocity of the acoustic wave. $p_g$ also denotes the internal pressure of the bubble which is modeled by van der Waals equation as shown in [17]:

$$p_g = \frac{N_{tot}(t)kT}{\left[\frac{4\pi}{3}\left(R^3(t)-h^3\right)\right]} \quad (3)$$

In Eq. (3), $N_{tot}$ is the total number of molecules in the bubble including TG (Triglyceride), DG (DiGlyceride), MG (MonoGlyceride), G (Glycerol), FAME (Free fatty Acid Methyl Ester) and MeOH (Methanol), which varies according to evaporation, diffusion, condensation, reaction, temperature and time. $k$ and $h$ also represent the Boltzmann constant and van der Waals hard-core radius of various species in the bubble.

### 3.2. Energy balance

Temperature is determined by the energy balance over the cavitation bubble. The energy balance is approximated by considering

**Table 3**
Run numbers and biodiesel specifications.

| Run | Micro mixing | | | | | Macro mixing | | | | |
|---|---|---|---|---|---|---|---|---|---|---|
| | $\rho$ kg/m$^3$ | $\mu$ mm$^2$/sec | CP °C | PP °C | FP °C | $\rho$ kg/m$^3$ | $\mu$ mm$^2$/s | CP °C | PP °C | FP °C |
| 1 | 875.8 | 4.467 | 14 | 10 | 204.5 | 876.1 | 4.56 | 14.5 | 11 | 206.5 |
| 2 | 875.8 | 4.467 | 14 | 10 | 202.5 | 876 | 4.37 | 14.5 | 11 | 202.5 |
| 3 | 875.7 | 4.391 | 14 | 10 | 196.5 | 876 | 4.37 | 14.5 | 11 | 202.5 |
| 4 | 875.5 | 3.833 | 13.5 | 8.5 | 194.5 | 875.9 | 4.31 | 13.0 | 10.5 | 198.5 |
| 5 | 875.8 | 4.244 | 14 | 9.5 | 192.5 | 876 | 4.44 | 14.0 | 11 | 204.5 |
| 6 | 875.5 | 3.955 | 13.5 | 9 | 188.5 | 875.9 | 4.30 | 13.5 | 10.5 | 198.5 |
| 7 | 875.6 | 4.148 | 13.5 | 9 | 190.5 | 875.9 | 4.30 | 13.5 | 10.5 | 198.5 |
| 8 | 875.5 | 3.987 | 13 | 9 | 188.5 | 875.7 | 4.14 | 13.5 | 10 | 194.5 |
| 9 | 875.7 | 4.367 | 14 | 10 | 196.5 | 876.1 | 4.47 | 14.5 | 11 | 206.5 |
| 10 | 875.6 | 4.167 | 13.5 | 9.5 | 192.5 | 875.8 | 4.33 | 14.0 | 10.5 | 198.5 |
| 11 | 875.7 | 4.256 | 14 | 9.5 | 194.5 | 875.9 | 4.35 | 14.0 | 11 | 200.5 |
| 12 | 875.5 | 3.765 | 13 | 8.5 | 192.5 | 875.7 | 4.15 | 13.0 | 10 | 194.5 |
| 13 | 875.8 | 4.172 | 13.5 | 9.5 | 192.5 | 875.9 | 4.30 | 14.0 | 10.5 | 200.5 |
| 14 | 875.5 | 3.883 | 13 | 8.5 | 188.5 | 875.7 | 4.15 | 13.0 | 10 | 194.5 |
| 15 | 875.5 | 3.782 | 13.5 | 8.5 | 188.5 | 875.8 | 4.24 | 13.0 | 10.5 | 198.5 |
| 16 | 875.5 | 3.833 | 13 | 9 | 188.5 | 875.7 | 4.15 | 13.5 | 10 | 194.5 |
| 17 | 875.7 | 4.283 | 13.5 | 9.5 | 194.5 | 875.8 | 4.24 | 14.0 | 10.5 | 198.5 |
| 18 | 875.6 | 4.148 | 13.5 | 9 | 190.5 | 875.8 | 4.21 | 13.5 | 10.5 | 196.5 |
| 19 | 875.6 | 4.130 | 13.5 | 9 | 190.5 | 875.8 | 4.16 | 13.5 | 10.5 | 196.5 |
| 20 | 875.4 | 3.833 | 13 | 8.5 | 188.5 | 875.7 | 4.09 | 13.0 | 10 | 192.5 |
| 21 | 875.8 | 4.132 | 13.5 | 9 | 190.5 | 875.8 | 4.23 | 13.5 | 10.5 | 198.5 |
| 22 | 875.4 | 3.819 | 13 | 8.5 | 186.5 | 875.7 | 4.09 | 13.0 | 10 | 192.5 |
| 23 | 875.6 | 4.171 | 13.5 | 9.5 | 192.5 | 875.8 | 4.17 | 14.0 | 10.5 | 196.5 |
| 24 | 875.5 | 3.922 | 13 | 8.5 | 188.5 | 875.6 | 4.01 | 13.0 | 10 | 188.5 |
| 25 | 875.6 | 4.153 | 13 | 9.5 | 192.5 | 875.7 | 4.09 | 14.0 | 10 | 192.5 |
| 26 | 875.5 | 4.008 | 13 | 9 | 188.5 | 875.6 | 4.04 | 13.5 | 10 | 190.5 |
| 27 | 875.6 | 4.121 | 13 | 9 | 190.5 | 875.7 | 4.09 | 13.5 | 10 | 192.5 |
| 28 | 875.4 | 3.783 | 12.5 | 8.5 | 188.5 | 875.5 | 4.05 | 13.0 | 9.5 | 188.5 |
| 29 | 875.8 | 4.257 | 13 | 9.5 | 194.5 | 875.6 | 4.07 | 14.0 | 10 | 190.5 |
| 30 | 875.4 | 3.783 | 13 | 8.5 | 186.5 | 875.6 | 4.03 | 13.0 | 10 | 188.5 |
| 31 | 875.5 | 4.003 | 13 | 9 | 188.5 | 875.6 | 4.07 | 13.5 | 10 | 190.5 |
| 32 | 875.4 | 3.783 | 12 | 8.5 | 186.5 | 875.5 | 3.94 | 13.0 | 9 | 186.5 |
| 33 | 875.7 | 4.257 | 13.5 | 9.5 | 194.5 | 875.9 | 4.30 | 14.0 | 10.5 | 200.5 |
| 34 | 875.4 | 3.783 | 13.5 | 8.5 | 186.5 | 875.8 | 4.20 | 13.0 | 10.5 | 196.5 |
| 35 | 875.7 | 4.322 | 13.5 | 9.5 | 194.5 | 875.8 | 4.28 | 14.0 | 10.5 | 198.5 |
| 36 | 875.5 | 4.057 | 13.5 | 9 | 188.5 | 875.8 | 4.17 | 13.5 | 10.5 | 196.5 |
| 37 | 875.6 | 4.181 | 13.5 | 9.5 | 192.5 | 875.8 | 4.16 | 14.0 | 10.5 | 198.5 |
| 38 | 875.6 | 4.130 | 13.5 | 9 | 190.5 | 875.8 | 4.21 | 13.5 | 10.5 | 196.5 |
| 39 | 875.6 | 4.162 | 14 | 9.5 | 192.5 | 875.9 | 4.35 | 14.0 | 11 | 202.5 |
| 40 | 875.6 | 4.119 | 13.5 | 9 | 190.5 | 875.8 | 4.18 | 13.5 | 10.5 | 196.5 |
| 41 | 875.7 | 4.357 | 14 | 10 | 196.5 | 876 | 4.41 | 14.5 | 11 | 204.5 |
| 42 | 875.6 | 4.098 | 13 | 9 | 190.5 | 875.7 | 4.14 | 13.5 | 10 | 194.5 |
| 43 | 875.6 | 4.193 | 13.5 | 9.5 | 192.5 | 875.8 | 4.19 | 14.0 | 10.5 | 198.5 |

the heat transfer across the bubble ($dQ/dt$); the rate of work done by the bubble ($P_i dV$) which is reduced during the expansion phase and the varying rate of number of molecules within the bubble ($dN_S/dt$). Therefore, the energy balance is introduced as:

$$C_{v,\mathrm{mix}}\frac{dT}{dt}=\frac{dQ}{dt}-P_i dV+(h_s-U_s)\frac{dN_s}{dt} \tag{4}$$

where $h_s$ and $U_s$ are the molecular enthalpy and internal energy of each compound. $C_{v,\mathrm{mix}}$ represents the specific heat of the mixture that can be obtained by the molecular specific heat of each compound and the number of its molecules $\sum_{i=1}^{N} C_{v,i}N_i$:

$$C_{v,i}=N_i k\left(\frac{f_i}{2}+\sum\frac{(\theta_i/T)^2\exp(\theta_i/T)}{(\exp(\exp(\theta_i/T)-1)^2)}\right) \tag{5}$$

In Eq. (5), $\theta_i$ denotes the vibrational temperature of each compound which provides information on energy transfer between the electrons and heavy particles, especially molecules, and can be obtained by:

$$\theta_i=\frac{h\cdot v}{k_B} \tag{6}$$

$v$ represents the wave number and the related values are given in Table 4

**Table 4**
Vibrational temperatures of various species.

| Species | Characteristic wave number | | | | |
|---|---|---|---|---|---|
| Triglyceride | 1713 | 1745 | 1734 | | |
| Diglyceride | 1713 | 1559 | 2915 | | |
| Monoglyceride | 1713 | 1733 | 1745 | | |
| Gelycerol | 919 | 1040 | 1120 | 1410 | 1474 |
| | 1565 | 1656 | 2914 | 3025 | 3308 |
| FAME | 722 | 1117 | 1159 | 1378 | |
| | 1464 | 1743 | 2852 | 2920 | |

### 3.3. Heat transfer

Conductive heat transfer across the bubble wall is determined analogously with mass transfer by Eqs. (7) and (10) respectively:

$$\frac{dQ}{dt}=4\pi R^2\kappa\left(\frac{T_0-T}{l_{\mathrm{th}}}\right),\ l_{\mathrm{th}}=\min\left(\sqrt{\frac{R\chi}{|dR/dt|}},\frac{R}{\pi}\right) \tag{7}$$

where $T$ and $T_0$ are the temperature of bubble contents and bubble wall, respectively. $\kappa$ is the thermal conductivity of the bubble contents that can be obtained by the following equation:

$$\kappa_{mix} = \sum_i \frac{\xi_i \kappa_i}{\sum_j \xi_j \Phi_{i,j}}, \tag{8}$$

$$\Phi_{i,j} = \frac{1}{\sqrt{8}}\left(1+\frac{m_i}{m_j}\right)^{-1/2}\left[1+\left(\frac{\eta_i}{\eta_j}\right)^{-1/2}\left(\frac{m_j}{m_i}\right)^{1/4}\right]^2 \tag{9}$$

where $m_i$, $\eta_i$, $\xi_i$ are the molecular mass, viscosity and the mole fraction of species $i$. The thermal diffusivity is eventually obtained from $\chi = \kappa_{mix}/c_p$. $l_{th}$ is also the thermal diffusion thickness.

### 3.4. Mass transfer

The mass-transfer effect which is critically influenced by $N_{tot}$, is obtained by employing the bubble dynamic and diffusion equations along with the reaction. Generally, the vapor transport is a two-step process, consisting of diffusion to the wall and condensation. However, the transport phenomena layer is more controlled by diffusion rather than condensation [18]. Therefore, the diffusion-limited model of the boundary layer approach proposed by Toegel et al. [19] was used in this study:

$$\frac{dN_{d,i}}{dt} = 4\pi R^2 D \left.\frac{\partial n}{\partial r}\right|_{r=R} \approx 4\pi R^2 D\left(\frac{n_{i,0}-n_i}{l_d}\right),\ l_d = \min\left(\sqrt{\frac{RD}{|dR/dt|}}, \frac{R}{\pi}\right) \tag{10}$$

where $n_{i,0}$ and $n_i$ are the equilibrium and instantaneous concentration of molecules of compound $i$, respectively. $D$ represents the binary diffusion coefficient and $l_d$ represents the instantaneous diffusive penetration depth. Diffusion coefficients are also approximated for each species by employing the model of Wilke and Chang [18]. Since methanol was used excessively in the reaction mixture in this study, the diffusivity of all other compounds in methanol was considered:

$$D_{i,MeOH} = 7.4\times10^{-8}\frac{\sqrt{\Phi_{MeOH}M_{MeOH}}T}{\eta_{MeOH}v_i^{0.6}} \tag{11}$$

where, $\Phi_{MeOH}$, $M_{MeOH}$ and $\eta_{MeOH}$ represent the association factor, molecular weight (g mol$^{-1}$) and viscosity of methanol (cP) respectively. $v_i$ also denotes the molar volume of species $i$ at its normal boiling temperature (cm$^3$ mol$^{-1}$).

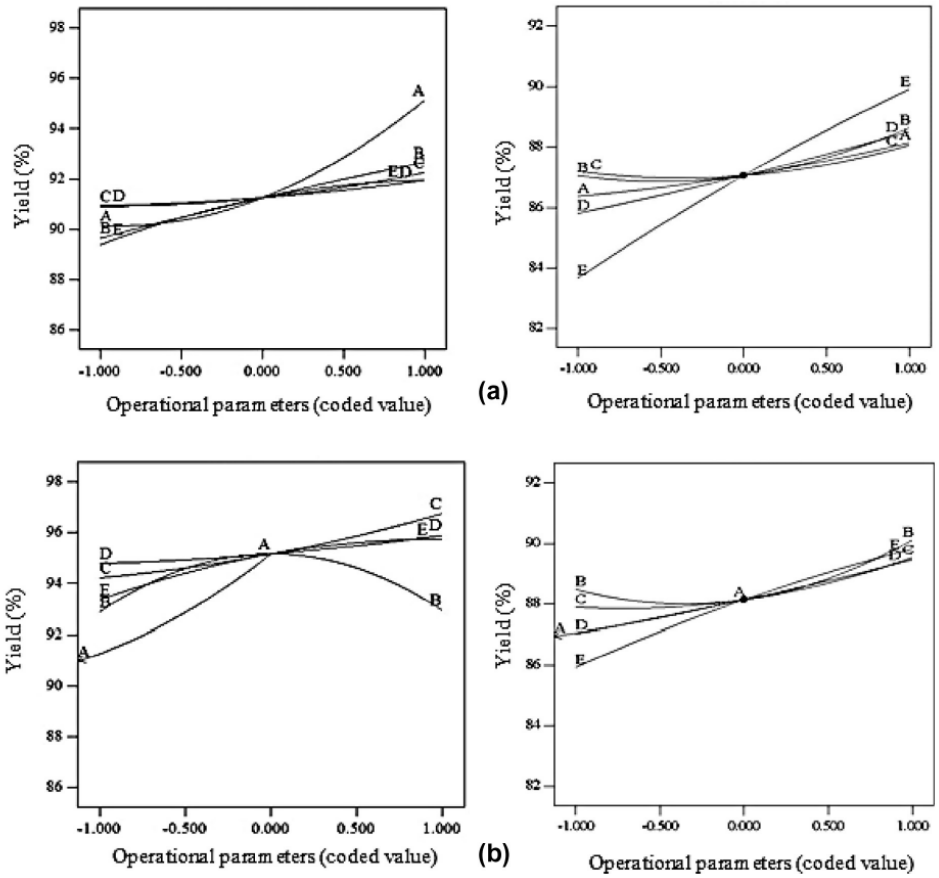


**Fig. 1.** Perturbation graph of reaction yeild at the temperature of (a) 57 °C, (b) 64 °C A: temperature, (°C), B: MeOH:oil (molar ratio), C: catalyst concentration (wt.%), D: sonication power (W), E: time (min): left: US, right: CS.

### 3.5. Chemical reactions

The values of the reaction rate constants which exactly match this work were obtained from the related literature [20]. However, the kinetics of the reactions inside the cavitation bubble were several orders of magnitude higher than the time scale of bubble dynamics due to very high temperature within the bubbles [21]. Therefore, the well-known Arrhenius law was employed to describe the net reaction rates per unit volume within the cavitation bubble:

$$r_j = k n_{tot} n_i n_j T \times \exp\left(-\frac{E_{f,i}}{kT}\right) \quad (12)$$

By considering Eqs. (10) and (12) for diffusion and chemical reaction, the total changes in the number of molecules for each species is expressed by:

$$\frac{dN_i}{dt} = \frac{dN_{d,i}}{dt} + \frac{dN_{R,i}}{dt} \quad (13)$$

The set of ODEs in the bubble dynamics model can be solved simultaneously using the well-known Runge–Kutta adaptive step size method.

Generally, a single sonoluminescence bubble in the reactant mixture is described under the conditions of reaction. The mathematical analysis was carried out with the assumptions on compressible boundary conditions. The parameters and constants of the mixture were fixed accordingly based on Table 5.

It worth noting that, such method of analyzing were employed by Kuppa et al. [22] and Choudhury et al. [23] firstly.

## 4. Result and discussion

### 4.1. Experimental results

#### 4.1.1. Reaction yield

Table 2 and Fig. 1 present the experimental results of reaction yield for both ultrasound assisted transesterification and traditional macro mixing with conventional heating. Although investigation of reaction yield is not the major scope of this work, it is presented to clarify the other sections. As mentioned earlier, an ultrafine mixing is generated under ultrasound irradiation which leads to major mass transfer between the reactants. Therefore, the maximum yield of 93.84% was achieved in just about 20 min at MeOH:oil molar ratio of 6:1 (Run No. 14). Meanwhile, the reaction reached only 89.09% in the same condition with mechanical stirring and conventional heating. By further increasing the reaction time to 60 min under ultrasonication, the reaction reached 95.44% (Run No. 30) and 95.71% (Run No. 32) at the MeOH:oil molar ratio of 6:1 and 12:1 respectively. However, the maximum yield of 94.01% (Run No. 32) was achieved with mechanical stirring performed at the maximum values of all parameters. Generally, temperature was the most effective parameter in both methods (Fig. 1) while mixing intensity and time exerted more influence on the reaction under mechanical stirring (Figs. 1 and 2). In other words, a fine mico-emulsion was produced under ultrasound irradiation even with the lowest power; the reaction therefore slightly increased at higher sonication intensity. Another noteworthy point is presence of sufficient amount of alcohol had a noticeable impact on the reaction yield under traditional heating. The reaction yield

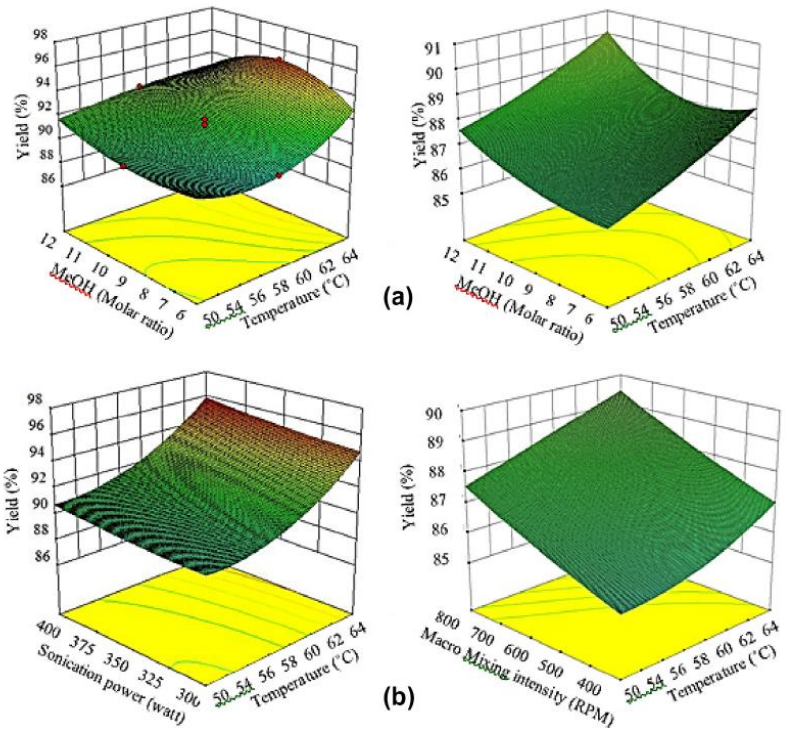


**Fig. 2.** Response surface of reaction yield versus temperature and (a) MeOH:oil molar (b) reactor power at the middle value of other parameters: left: US, right: CS.

increased by increasing MeOH:oil molar ratio up to 9 under ultrasound and it then reached a plateau by further increase in alcohol concentration. It dramatically reduced at higher MeOH:oil molar ratio and temperature (above 59 °C) (Fig. 2). The reason is increasing the methanol quantity till an optimum value leads to increase of cavitational intensity, formation of smaller drop sizes (higher emulsion quality) and provision of extra areas for mass transfer which eventually increases conversion. Beyond that, excessive methanol reduces the concentrations catalyst as well as interfacial area due to smaller volume of oil in reaction mixture. In general, the reaction yield produced under ultrasound irradiation was 3.69% higher than that produced by conventional heating under similar production conditions.

*4.1.2. Biodiesel characterization*

Table 3 and Figs. 3 and 4 compare the physicochemical properties of biodiesel produced by sonoluminescence micro and stirring macro synthesis. Based on the table, the produced biodiesel by both systems fully conform to the range given in both ASTM and EN, except for 5 runs of traditional conventional heating, which did not conform to the pour point standard.

In this study, the biodiesel samples produced by ultrasonication power had slightly lower densities and viscosities than those produced by traditional heating under the same operational conditions. The maximum density of 876.1 kg/m$^3$ was observed in the case of CSR (Run No. 1), while the maximum density of 875.8 kg/m$^3$ was achieved in cases of UAR (Runs No. 1, 2, 5, 13, 21, 29, US). Furthermore, the viscosity of biodiesel produced under ultrasound irradiation was about 0.12 mm$^2$/s lower than that produced under traditional conventional heating. The viscosity of biodiesel produced by ultrasound in this work was also lower compared to that produced by the other methods [24–27]. In terms of cold flow properties, the minimum and maximum cloud point observed were 12, the minimum an UAR) and 14.5 °C (Run No. 1, 2, 3) respectively while the minimum and maximum pour point observed were 8.5 °C (Runs with the greatest yield US) and 11 °C (Runs with the least reaction yield CON) respectively. Furthermore, ultrasound decreased pour point by nearly 1~2 ℃. However, no significant improvement in cloud point was observed. Besides, the cold flow properties obtained under ultrasound irradiation in this work were nearly 5° lower than those produced by other conventional methods [11–16,18–21]. As summarized in Table 3, the flash point of all biodiesel samples was much greater than expected based on ASTM D93-07. However, the flash point of biodiesel produced by ultrasound waves was slightly lower than that produced by mechanical stirrer and conventional heating. The same observation in terms of biodiesel properties was also reported by Salamatinia et al. [28].

Analysis of the sample with the highest viscosity/density/flash point showed that it contained 32.86% of C16:0; 3.67% of C18:0; 35.06% of C18:1 and 9.67%. of C18:2. On the other hand, the average compositions of less viscous/dense samples were 33.75% of C16:0; 3.81% of 5C18:0; 36.48% of C18:1 and 10.16% of C18:2.

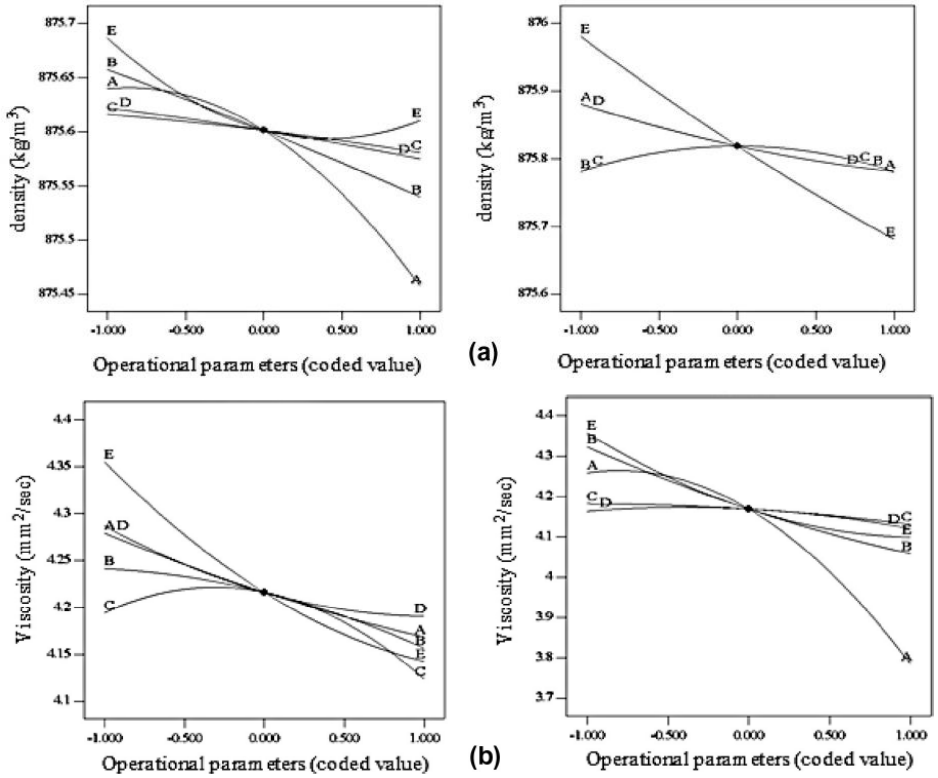


**Fig. 3.** Perturbation graph of (a) density, (b) viscosity A: temperture, (°C), B: MeOH:oil (molar ratio), C: catalyst concentration (wt.%), D: sonication power (W), E: time (min): left: US, right: CS.

Therefore, the content of triglycerides in the samples has more influence on the biodiesel properties compared to the content of saturated and unsaturated components in biodiesel. In other words, the samples with higher amount of unreacted triglyceride presented greater values for each property. The same flow pattern was also observed for cold flow properties. Therefore, the pour and cloud point increased in samples with higher amount of unreacted triglycerides. The reason is triglycerides (especially in palm oil) are huge molecules with three branches. At low temperature, the branches are stuck in each other and inhibit further molecular motions. This phenomenon is more prominent in palm oil biodiesel due to its long carbon chain ($C_{16}$–$C_{18}$) [29]. Hence, the samples with higher reaction yield presented lower values for each property (which is also more favorable).

According to Analysis of Variance, a statistical analysis, all operational parameters except catalyst concentration showed positive influence on biodiesel properties in both cases. However, MeOH:oil molar ratio was more effective for the US samples. It is because greater alcohol concentration till an optimum value increases the cavitational intensity and formation of smaller drop sizes. This condition leads to higher emulsion quality, providing extra area for mass transfer and increasing the reaction yield subsequently.

Mixing intensity and time are more important for the CON samples. This is due to the necessity for a better mixing and contact time between the reactants in the mechanical stirring system to obtain better yield. Reaction temperature was also the most effective parameter in both cases. It is clear that the biodiesel properties were affected by reaction yield. Hence, the pattern of biodiesel properties changes and reaction yield were similar, based on comparison of Figs. 3 and 4 with Fig. 1. More details about the interaction and other influences of operational parameters are observed in Figs. 3 and 4.

The other point that should be highlighted is related to decomposition reactions. As mentioned earlier, such reactions may be activated at extremely high reaction temperatures and pressures. The mathematical modeling may clarify the mechanistic features of sonoluminescence bubbles and develop a link between the bubbles properties and decomposition reactions.

### 4.2. Numerical analysis

Figs. 5a–e present the simulation results of the sonoluminescence bubble characteristics, which included radius, temperature,

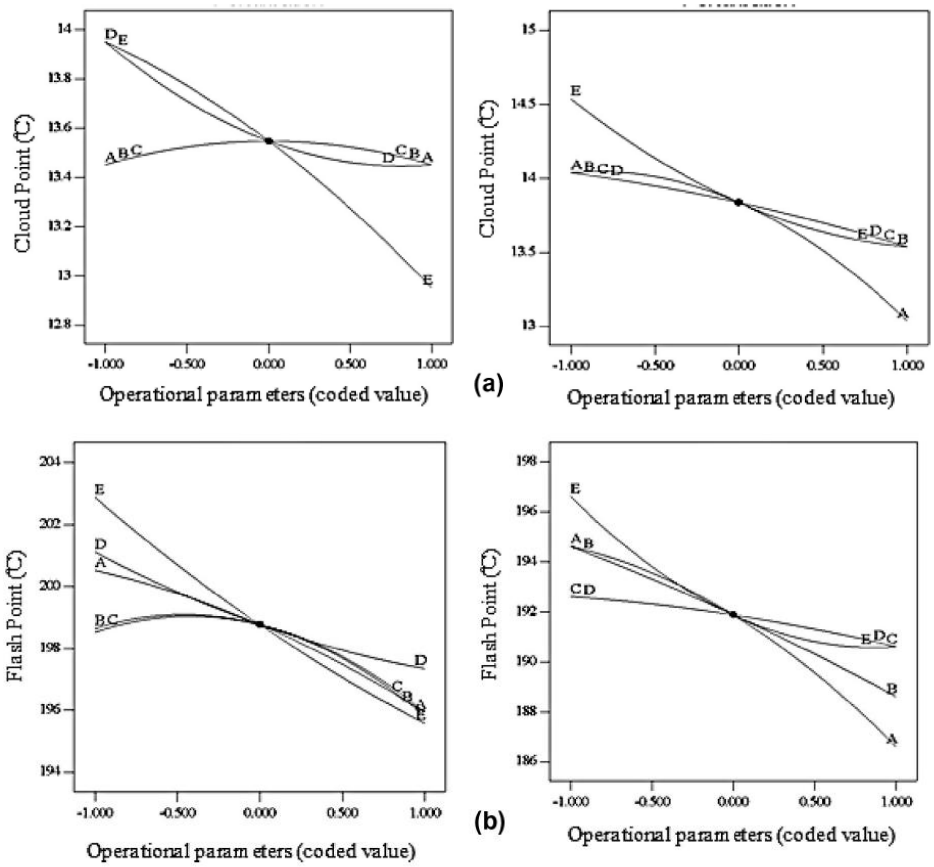


**Fig. 4.** Perturbation graph of (a) cloud point, (b) flash point A: temperture, (°C), B: MeOH:oil (molar ratio), C: catalyst concentration (wt.%), D: sonication power (W), E: time (min): left: US, right: CS.

Link to Full-Text Articles :

***http://www.sciencedirect.com/science/article/pii/S1350417714001904***